

Gliomas: Motexafin Gadolinium-enhanced Molecular MR Imaging and Optical Imaging for Potential Intraoperative Delineation of Tumor Margins¹

Longhua Qiu, PhD, MD
 Feng Zhang, PhD, MD
 Yaoping Shi, PhD, MD
 Zhibin Bai, MD
 Jianfeng Wang, PhD, MD
 Yonggang Li, MD, PhD
 Donghoon Lee, PhD
 Christopher Ingraham, MD
 Xiaoyuan Feng, PhD, MD
 Xiaoming Yang, PhD, MD

Purpose:

To investigate the possibility of using motexafin gadolinium (MGd)-enhanced molecular magnetic resonance (MR) imaging and optical imaging to identify the true margins of gliomas.

Materials and Methods:

The animal protocol was approved by the institutional animal care and use committee. Thirty-six Sprague-Dawley rats with gliomas were randomized into six groups of six rats. Five groups were euthanized 15, 30, 60, 120, and 240 minutes after intravenous administration of 6 mg/kg of MGd, while one group received only saline solution as a control group. After craniotomy, optical imaging and T1-weighted MR imaging were performed to identify the tumor margins. One-way analysis of variance was used to compare optical photon intensity and MR imaging signal-to-noise ratios. Histologic analysis was performed to confirm the intracellular uptake of MGd by tumor cells and to correlate the tumor margins delineated on both optical and MR images.

Results:

Both optical imaging and T1-weighted MR imaging showed tumor margins. The highest optical photon intensity (2.6×10^8 photons per second per $\text{mm}^2 \pm 2.3 \times 10^7$; analysis of variance, $P < .001$) and MR signal-to-noise ratio (77.61 ± 2.52 ; analysis of variance, $P = .006$) were reached at 15–30 minutes after administration of MGd, with continued tumor visibility at 2–4 hours. Examination with confocal microscopy allowed confirmation that the fluorescence of optical images and MR imaging T1 enhancement exclusively originated from MGd that accumulated in the cytoplasm of tumor cells.

Conclusion:

MGd-enhanced optical and MR imaging can allow determination of glioma tumor margins at the optimal time of 15–120 minutes after administration of MGd. Clinical application of these results may allow complete removal of gliomas in a hybrid surgical setting in which intraoperative optical and MR imaging are available.

©RSNA, 2015

¹From the Image-Guided Biomolecular Intervention Research, Department of Radiology, University of Washington School of Medicine, 850 Republican St, Seattle, WA 98109 (L.Q., F.Z., Y.S., Z.B., J.W., Y.L., D.L., C.I., X.Y.); and Department of Radiology, Huashan Hospital, Fudan University, Shanghai, China (L.Q., X.F.). Received April 22, 2015; revision requested June 10; revision received August 4; accepted August 11; final version accepted August 27. Address correspondence to X.Y. (e-mail: xmyang@u.washington.edu).

L.Q. and F.Z. contributed equally to this work.

©RSNA, 2015

Gliomas are the most common primary brain tumors. The prognosis of patients with high-grade gliomas remains extremely poor, with a median survival of only 12–15 months from the time of diagnosis (1,2). Current treatment strategies for gliomas include surgical resection and combined radiation therapy and chemotherapy, which only extend survival by a few months (3). The extent of gross total resection of gliomas with the goal of achieving maximal tumor resection with the least postoperative neurologic deficits has been a critical factor in survival (3–5). However, gliomas have a high propensity to infiltrate along white matter tracts, sometimes to considerable distances from the edge of the gross tumor (6,7). This factor can make complete resection of tumors extremely challenging with conventional imaging-based microsurgical techniques (5). This difficulty is in part due to limitations of conventional imaging techniques to accurately

distinguish glioma infiltration from normal brain tissue (5). Therefore, it is imperative to develop intraoperative imaging-guided techniques that can ensure identification of tumor margins to allow complete tumor removal (8).

Recent advances in imaging-guided techniques for glioma resection include intraoperative magnetic resonance (MR) imaging (9–12) and three-dimensional ultrasonographic (US) imaging (13). Both of these imaging techniques can provide cross-sectional and three-dimensional information and depict the depth of the tumor under the cortical surface. This improves tumor visualization during surgery and allows for more complete tumor resection (13). Fluorescence-guided resection with 5-aminolevulinic acid also has been used as a promising tool in localizing tumors and guiding resection (5,13–15). However, each of these modalities has inherent limitations and disadvantages. Three-dimensional US can easily create artifacts, causing its accuracy to decrease as the surgery progresses (13). Intraoperative MR imaging is typically performed after the administration of paramagnetic contrast agent, which is an extracellular agent. This poses the potential problem of obscuring tumor margins if the contrast agent leaks from a vessel that has been opened surgically (10). As an alternative, visualization with fluorescence is essentially a surface imaging technique, with limited depth penetration (13,16). Therefore, recent efforts have been made to integrate intraoperative MR imaging with optical imaging in one surgical setting, combining the advantages of two imaging modalities: high soft-tissue contrast and spatial resolution with MR imaging and high sensitivity and real-time data acquisition with optical imaging (17).

The feasibility of this combination is reliant on the availability of an intracellular MR and optical imaging marker. Once a reliable imaging marker is available, simultaneous intraoperative dual-modality imaging can guide the resection of complex brain tumors, such as gliomas.

Motexafin gadolinium (MGd), a porphyrin-like molecule that has been used in clinical trials, functioning as a radiation and chemotherapy sensitizer, an intracellular T1-weighted MR imaging enhancer, and a red fluorescence emitter (18). Results of previous studies (19–22) have confirmed that MGd can be internalized exclusively in metabolically active tissues, such as atherosclerotic plaques and different tumors. It also can cross the disrupted blood-brain barrier associated with brain tumors, but it is not detectable in normal brains (18,23,24). The aim of this study was to investigate the possibility of using MGd-enhanced molecular MR imaging and optical imaging to identify the true margins of gliomas.

Advances in Knowledge

- Glioma tumor cells take up motexafin gadolinium (MGd) in a time- and concentration-dependent fashion, with the earliest intracellular accumulation at 15–30 minutes and an optimal concentration of 100 $\mu\text{g}/\text{mL}$ after the addition of MGd.
- Both optical and MR imaging demonstrated the highest photon signal intensity (2.6×10^8 photons per second per $\text{mm}^2 \pm 2.3 \times 10^7$; analysis of variance, $P < .001$) and MGd enhancement (signal-to-noise ratio, 77.61 ± 2.52 ; analysis of variance, $P = .006$) at 15–30 minutes after MGd administration, with continued visibility lasting for 2–4 hours.
- Histologic analysis allowed confirmation that the fluorescence of optical images and MR imaging T1 enhancement originated exclusively from MGd that accumulated in the cytoplasm of tumor cells.



Implication for Patient Care

- Intraoperative integration of MGd-enhanced molecular optical imaging and MR imaging allows for the potential clinical benefit of guiding complete removal of human gliomas in one hybrid surgical setting.

Materials and Methods

MGd was provided by Pharmacyclics (Sunnyvale, Calif). The authors had full

Published online before print

10.1148/radiol.2015150895 Content codes:  

Radiology 2016; 279:400–409

Abbreviation:

MGd = motexafin gadolinium

Author contributions:

Guarantors of integrity of entire study, L.Q., F.Z., Z.B., J.W., Y.L., X.Y.; study concepts/study design or data acquisition or data analysis/interpretation, all authors; manuscript drafting or manuscript revision for important intellectual content, all authors; approval of final version of submitted manuscript, all authors; agrees to ensure any questions related to the work are appropriately resolved, all authors; literature research, L.Q., Z.B., J.W., C.I., X.F.; clinical studies, Z.B., J.W.; experimental studies, L.Q., F.Z., Y.S., Z.B., J.W., Y.L., D.L.; statistical analysis, L.Q., F.Z., Z.B., J.W., X.Y.; and manuscript editing, L.Q., F.Z., Z.B., J.W., D.L., C.I., X.Y.

Funding:

This research was supported by the National Institutes of Health (grant R01EB012467).

Conflicts of interest are listed at the end of this article.

control of the data and the submitted information.

Study Design

This study was performed between December 2013 and February 2015. Our study included two phases: (a) *in vitro* experiments to investigate the feasibility of using optical imaging and molecular MR imaging to confirm and quantify the intracellular uptake of MGd by glioma cells, while determining the optimal concentration of MGd and incubation time; and (b) *in vivo* animal experiments to validate the feasibility of using combined molecular MR imaging and optical imaging to assess the real margins of MGd-illuminated gliomas in rat brains.

In Vitro Experiments

Cell culture.—Rat C6 glioma cells were seeded (5×10^4 per well) into four-well chamber plates (Laboratory Tek II; Thermo Fisher Scientific, Rochester, NH). Cells were maintained in Delbecco's modified Eagle's medium (HyClone Laboratories, Logan, Utah) supplemented with 10% fetal bovine serum (Sigma-Aldrich, St Louis, Mo) in an incubator at 37°C with a 5% carbon dioxide atmosphere.

Confocal microscopy of MGd-treated cells.—As cells were cultured to reach 80% confluence, MGd was added to yield final concentrations of 0, 25, 50, 75, 100, 125, 150, and 200 $\mu\text{g}/\text{mL}$. Cells were then cultured for an additional 24 hours. Six wells were prepared for each concentration. MGd-treated cells were then washed twice with phosphate-buffered saline to remove free MGd, were fixed in 4% paraformaldehyde, and were dried at room temperature. Cell plates were counterstained with 4', 6-diamidino-2-phenylindole (DAPI; Vector Laboratories, Burlingame, Calif) and then imaged with a laser confocal microscope (A1R; Nikon, Tokyo, Japan) to detect and compare the MGd-emitted red fluorescence in the cells at different MGd concentrations. To verify the time required for uptake of MGd by the cells, additional glioma cell groups were treated with MGd at 100 $\mu\text{g}/\text{mL}$ for 15 and 30 minutes and 1, 2, 4, 12,

24, and 48 hours for the respective concentration levels. A nontreated cell group served as a control group.

Optical imaging and MR imaging of MGd-treated cells.—Additional groups of cells were cultured and grown on 10-mm culture plates to reach 80% confluence, and then treated with MGd at 0, 25, 50, 75, 100, 125, 150, and 200 $\mu\text{g}/\text{mL}$ for 24 hours. Six plates were created for each concentration. Cells were then collected and rinsed twice with phosphate-buffered saline. MGd-treated cells (5×10^6) were diluted with 0.1 mL of phosphate-buffered saline and were dispersed into 0.2-mL Eppendorf tubes containing 1% agarose.

Fluorescent optical imaging of cell-containing agarose tubes was performed with an *in vivo* small animal optical and x-ray imaging system (Bruker Biospin; Bruker, Billerica, Mass). Cell-containing tubes were imaged with an excitation wavelength at 470 nm, emission wavelength with a 750 nm filter, a field of view of 19×19 mm, and exposure time of 30 seconds.

MR imaging of cell-containing agarose tubes was performed by using a 3.0-T MR imaging system (Achieva; Philips Healthcare, Best, the Netherlands) and a wrist coil (SENSE wrist four-element coil; Philips Healthcare). T1 mapping of cells was performed by using the Look-Locker sequence: repetition time msec/echo time msec, 6.9/4.4; flip angle, 10°; field of view, 100 mm; section thickness, 0.8 mm; matrix, 434×434 ; and number of signals acquired, four. T1-weighted images were acquired in the sagittal and transverse planes by using a spin-echo sequence, 550/12; flip angle, 90°; field of view, 100 mm; section thickness, 1 mm; matrix, 500×498 ; and number of signals acquired, eight.

To evaluate MGd uptake times, cells cultured in 10-mm petri dishes were treated with MGd at a concentration of 100 $\mu\text{g}/\text{mL}$ at varying incubation times of 15, 30, and 60 minutes and 2, 4, 12, 24, and 48 hours. MGd-treated cells (5×10^6) were collected, dispersed in 1% agarose tubes, and then imaged by using the optical imaging system and 3.0-T MR imager by using the same

imaging sequences and parameters as those previously described.

Imaging analysis.—Fluorescent signal intensity of MGd-treated cells was quantified by placing a 3-mm² region of interest at the center of cell-containing agarose tubes to measure photon quantities. The signal intensity of MGd-containing cells was plotted with MGd concentrations and incubation times to determine the optimal MGd dose and incubation time (F.Z., with 4 years of experience in optical imaging). MR images of MGd-treated cells were analyzed by measuring the signal intensity of cell-containing tubes. The signal intensity of each tube was measured by using the Digital Imaging and Communication in Medicine viewer (Philips DICOM Viewer R2.5 Version 1 Level 1; Philips Healthcare). A region of interest of 3 mm² was placed at the center of each tube by one radiologist (L.Q., with 5 years of experience in MR imaging).

Animal Experiments

Creation of rat models with brain gliomas.—The animal protocol was approved by our institutional animal care and use committee. Thirty-six male Sprague-Dawley rats (mean weight, 160 g \pm 20) were anesthetized by means of inhalation of 1%–3% isoflurane (Piramal Health care, Andhra, India) in oxygen. By means of a stereotactic approach, 1.5×10^6 glioma cells were injected into the right caudate nucleus (2.8 mm lateral and 1.0 mm anterior to the bregma, at a depth of 4.0 mm) through a 10- μL Hamilton syringe. Tumors were then allowed to grow for 2 weeks. Twelve non-tumor-bearing rats served as negative controls.

Optical imaging.—All tumor-bearing rats were randomized into six groups of six rats. After injection of MGd (6 mg/kg) via the tail veins into the animals of five groups, the animals in these groups were euthanized at 15, 30, 60, 120, and 240 minutes. The remaining group of rats (tumor bearing) was injected with only saline solution to serve as controls. Twelve normal rats (without brain tumors) were randomized into two control groups of six rats. One group received 6 mg/kg of intravenous

MGd and the other group received saline solution only. Tumor-free animals were euthanized at 15 minutes after MGd or saline solution administration. By means of craniotomy, whole-brain optical imaging (with 470/750-nm excitation and emission filter sets, 19×19 -cm field of view, 1.1 f-stop, 4×4 bin, and 30-second exposure time) was performed with the optical/x-ray imaging system to delineate the tumors.

MR imaging.—Whole rat brains were placed into 15-mL tubes filled with perfluoropolyether (Fomblin; Solvay solexis, West Deptford, NJ). Whole-brain axial T1-weighted MR imaging (T1-weighted and T2-weighted imaging were performed by using a 14-T vertical wide-bore MR Spectrometer with a microimaging coil [Bruker]). T1-weighted images were acquired by using a low-flip angle gradient-echo sequence with the following parameters: 213.9/2.0; field of view, 190×128 mm; matrix, 190×96 ; section thickness, 0.5 mm; and number of signals acquired, 20. T2-weighted images were acquired by using a multisection multiecho sequence: 3000/5.7; field of view, 190×128 mm; matrix, 190×96 ; section thickness, 0.5 mm; and number of signals acquired, one.

Imaging analysis.—For optical imaging, images were analyzed (F.Z., with 4 years of experiences in optical imaging) by using imaging analysis software (Bruker MI 7.1 SE; Bruker). Regions of interest were drawn manually to include the entire red fluorescence-illuminated tumors, while in the control group, regions of interest were drawn to include right frontal lobes. Photons in the tumors were then quantified. For molecular MR imaging, all images were analyzed (L.Q., with 5 years of MR imaging experience) by using Digital Imaging and Communications in Medicine viewer software (RadiAnt DICOM viewer 1.9; Medixant, Poznan, Poland). Signal intensity of tumors was measured by drawing four regions of interest (25 pixels each) over the peripheral zone of the tumors at the largest cross-sectional diameters. Then, the average signal intensity of each tumor (SI_T) was calculated. The signal intensity (SI_N)

and standard deviation (SD_N) of the background noise were also measured by placing a region of interest on the background of each image. Signal-to-noise ratios were calculated by using the following equation: $(SI_T - SI_N)/SD_N$. Optical photon intensity and MR imaging signal intensity were plotted with the time-to-create photon and signal intensity time curves.

Histologic evaluation.—After optical and MR imaging were performed, the brain was snap-frozen and cryogenically sectioned with sections 8–10 μ m thick. Sections of tumors were then taken at the point of largest diameter of the mass. These were then stained with either 4', 6-diamidino-2-phenylindole for confocal microscopy to confirm exclusive intracellular uptake of MGd by tumor cells or hematoxylin and eosin to define the histologic margins of tumors. These sections were correlated with their corresponding optical and MR images of the tumors at the largest mass diameters.

Statistical Analysis

All values including the average tumor sizes, fluorescent signal intensity, and signal-to-noise ratios were depicted as means \pm standard error of the mean. Statistical comparison for the photon and signal intensity of the tumors and tumor sizes or control region of interest among different study groups was performed by using one-way analysis of variance (SigmaStat 3.5; Systat Software, Chicago, Ill). When analysis of variance showed significance, comparisons between means were performed with a two-tailed indirect Student *t* test.

Results

In Vitro Experiments: Time- and Dose-dependent Uptake of MGd by Glioma Cells

Confocal microscopy showed that MGd-treated cells emitted red fluorescence in the cytoplasm, which was not seen in the control cells (those not treated with MGd) (Fig 1). For the group of cells treated with different concentrations of MGd, ranging from 25 to 200 μ g/mL, we found that, in the concentration

range of 25–100 μ g/mL, as the concentration of MGd increased, fluorescent signal intensity of cells also increased, while MR imaging T1 values decreased. When MGd concentration was greater than 100 μ g/mL, the fluorescence signal intensity and MR imaging T1 values plateaued (Fig 2). Confocal microscopy allowed confirmation of quick intracellular uptake of MGd after 15–30 minutes of incubation (Fig 3). Quantification of cells by means of optical imaging showed an increase of fluorescence signal intensity as incubation times increased, which plateaued after the 24-hour time point (Fig 3).

Animal Experiments

All tumor-bearing rats survived to the time of euthanasia. Statistical comparisons of the tumor sizes among groups showed that there was no significance ($4.5 \text{ mm} \pm 0.5$, $4.5 \text{ mm} \pm 0.3$, $4.9 \text{ mm} \pm 0.7$, $5.7 \text{ mm} \pm 0.6$, $5.9 \text{ mm} \pm 0.7$, $5.2 \text{ mm} \pm 0.6$, for the groups, respectively; one-way analysis of variance, $P = .525$). Both optical imaging and MR imaging allowed delineation of MGd-illuminated tumors and definition of the margins of these tumors, which correlated well with pathologic findings with hematoxylin and eosin staining (Fig 4). The exclusive accumulation of MGd in tumor cells further confirmed that MGd could be selectively taken up by tumor cells and thus could be used to outline the distinct boundary between the tumor and normal brain parenchyma.

In the evaluation of the kinetics of MGd throughout a 4-hour period, both optical and MR imaging showed that the highest photon signal (2.6×10^8 photons per second per $\text{mm}^2 \pm 2.3 \times 10^7$; analysis of variance, $P < .001$) and MGd enhancement occurred at 15–30 minutes after MGd administration (MR imaging signal-to-noise ratio, 77.61 ± 2.52 , analysis of variance, $P = .006$) (Fig 5). Even though MGd-enhancing tumors demonstrated visibility for up to 4 hours, tumor margins at optical imaging became indistinct and tumor enhancement at MR imaging attenuated during the observation time course. No statistical differences were found between the 15-minute and the 2-hour

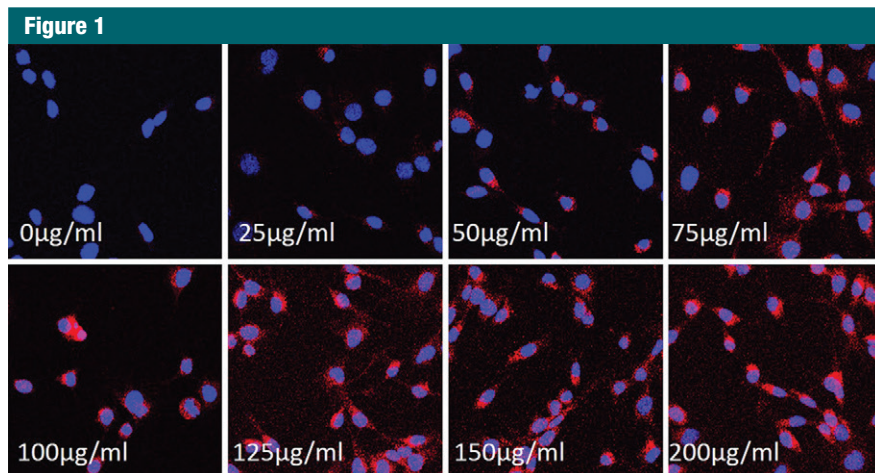


Figure 1: Confocal microscopic images of rat C6 glioma cells treated with MGd at different concentrations show that MGd-emitting red fluorescence signal intensity becomes more intense as concentration of MGd increases, which indicates that intracellular uptake of MGd is concentration dependent (magnification, $\times 20$).

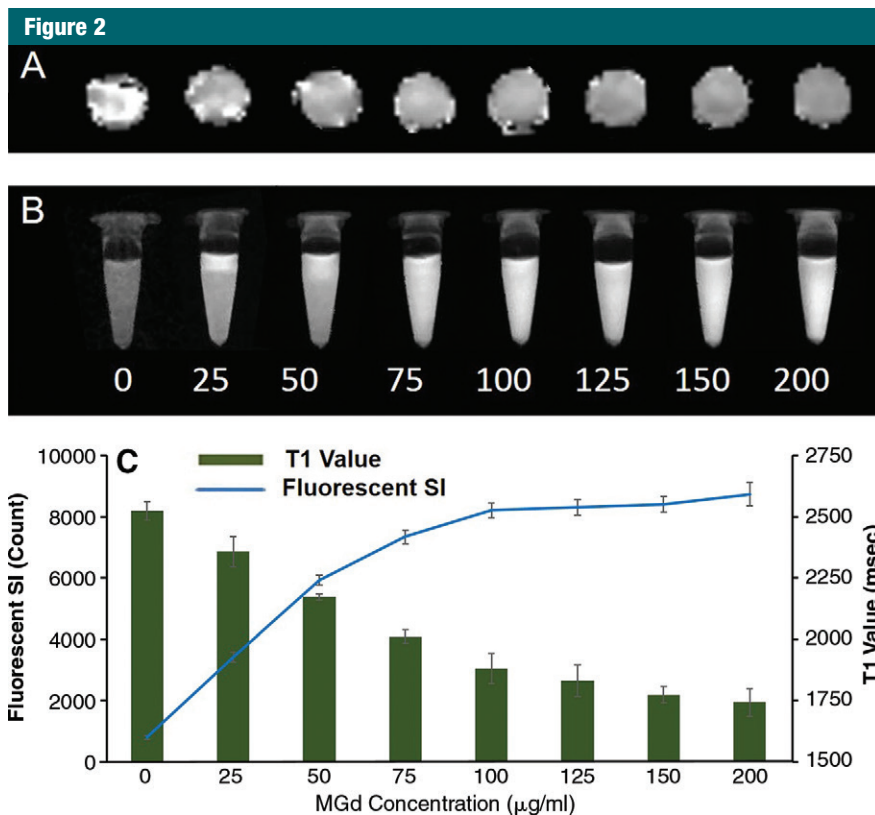


Figure 2: Quantitative analysis of cells treated with MGd at different concentrations. *A*, MR imaging T1 map of glioma cells and, *B*, fluorescent optical image of cells at different concentrations from 0 to 200 $\mu\text{g/ml}$ show that T1 value decreases and fluorescent signal (*SI*) increases as MGd concentrations increase. *C*, Graph shows T1 values and fluorescent signal compared with MGd concentration, further confirming that intracellular uptake of MGd increases as concentrations of MGd increase from 0 to 100 $\mu\text{g/ml}$ and then maintains stable level as MGd concentration increases further.

time points for either fluorescence or MR imaging signal intensity. Imaging findings correlated with results of confocal microscopy and hematoxylin and eosin-stained microscopy of the tumor tissues (Fig 6), which confirmed that tumor enhancement at optical and MR imaging originated from the intracellular location of MGd in tumor cells.

Discussion

In this preclinical study, we investigated the use of simultaneous MGd-based fluorescent optical imaging and MR imaging to outline the histologic margins of C6 gliomas in rats and to determine the optimal time window to visualize the tumors. Through in vitro experiments, we found the best concentration of MGd to be 100 $\mu\text{g/mL}$, which allowed for the maximal internalization of MGd by cells, with the earliest uptake noted at 15–30 minutes after the addition of MGd into the cell culture medium. For our in vivo experiments, we used a rat C6 glioma cell line to create the orthotopic glioma tumors, which tend to be morphologically similar to glioblastoma multiforme, in Sprague-Dawley rats. Fluorescent optical imaging and MR imaging were used to evaluate MGd-enhancing gliomas at different time points after the intravenous administration of MGd. Histologic analysis with confocal microscopy and hematoxylin and eosin staining microscopy on a section-by-section basis showed that at the boundary between normal brain tissue and tumor tissue, MGd had exclusively accumulated in the cytoplasm of tumor cells. The results from our animal experiments confirmed that fluorescent signal intensity and the enhancement on T1-weighted MR images peaked at 15–30 minutes after MGd injection. During the 4 hours when tumors were observed, tumors maintained their visibility with decreasing margin distinctions at both optical and MR imaging. These imaging findings were confirmed by subsequent pathologic correlations.

High-grade gliomas are among the most serious primary brain malignancies, which account for most brain

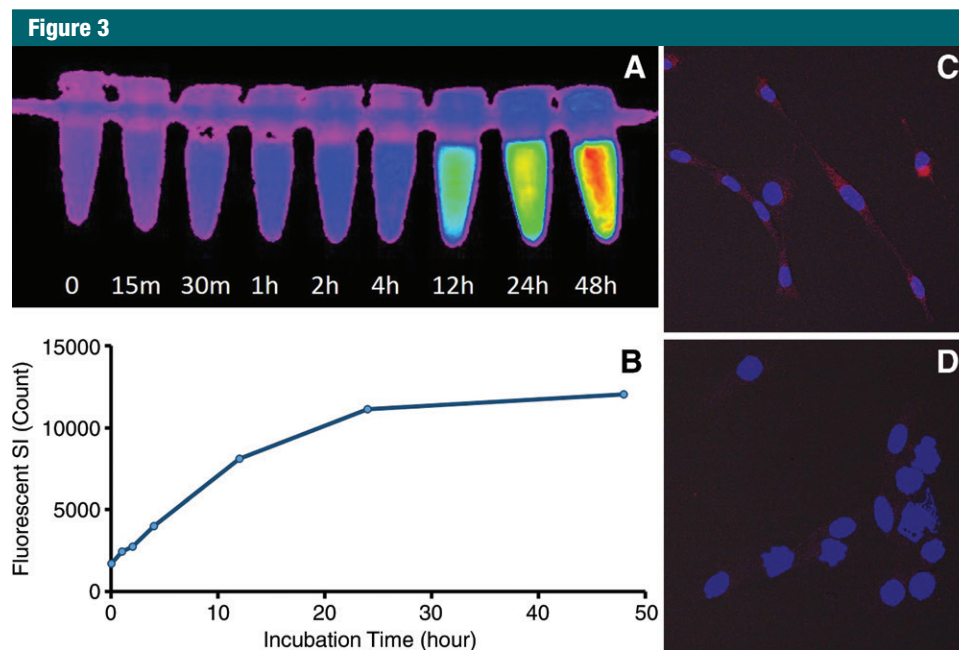


Figure 3: Optical imaging of cells treated with MGd at concentration of 100 $\mu\text{g/mL}$ at various incubation durations. *A*, Optical image shows that signal intensity (*SI*) of MGd-emitting fluorescence increases as MGd incubation time increases. *B*, Graph shows time to fluorescence signal intensity curve in which signal intensity increases from 0 to 24 hours and then plateaus for following 24 hours. *C*, Confocal microscopy confirms early uptake of MGd by cells after MGd incubation for 15 minutes, *D*, while no intracellular red fluorescence was seen in nontreated control cells (magnification, $\times 20$).

tumor-related deaths worldwide (1,2). To achieve the most durable long-term survival benefit for patients with gliomas, complete eradication of tumors while sparing the normal brain parenchyma remains the most challenging task for neurosurgeons (3,6,14,15). Because of this daunting task in patients with gliomas, numerous intraoperative imaging-guided surgical techniques have been developed in an effort to extend survival and improve quality of life (5,6,12,25,26). Use of a single imaging modality to guide surgery has inherent limitations and disadvantages. Surgery performed on the basis of the 5-aminolevulinic acid signal without functional data—especially in the vicinity of eloquent brain areas—could result in excess resection at the cost of increased risk of postoperative neurologic deficits (3). To date, intraoperative MR imaging involves the use of a conventional contrast agent such as gadopentetate dimeglumine (11,12). However, this gadolinium chelate may exude through

a glioma-compromised blood-brain barrier and accumulate in the extracellular space, which may lead to the pseudoenhancement of the adjacent normal brain tissues and thereby lead to further, unnecessary resection (9,18). To resolve these potential issues, new dual-modality MR imaging and optical imaging probes were developed to bridge these two distinctive but complementary imaging modalities with the intent of improving intraoperative imaging-guided surgery (9,27). In this context, MR imaging offers three-dimensional visualization of brain anatomy at high spatial resolution appropriate for presurgical planning, while optical imaging provides real-time intraoperative imaging for precise outlining of the margins of tumors being resected. However, these MR imaging and optical imaging probes still remain in their *in vitro* and *in vivo* experimental stages.

MGd has been used in clinical trials as a radiation and chemotherapy sensitizer (23,28–30), an intracellular

T1-weighted MR imaging contrast agent, and a red fluorescence emitter (19–21). In the current study, we attempted to investigate the application of MGd for intraoperative imaging-guided complete glioma resection. The results of our study show that MGd can allow delineation of the glioma tumor margins at an early time point after intravenous administration. Tumor visibility can last up to 4 hours at both fluorescent optical imaging and MR imaging because of the exclusive accumulation of MGd in tumor cells. The results of this study suggest that MGd has the promising potential to function as an ideal intracellular contrast agent for use in intraoperative optical and MR imaging with tumor specificity and intracellular localization. We also found that the peak enhancement of tumors occurred at 15–30 minutes after MGd administration. As observation time increased, the visible margins of the tumors decreased. As time progressed, the tumors became less visible because of the slow clearance of MGd from

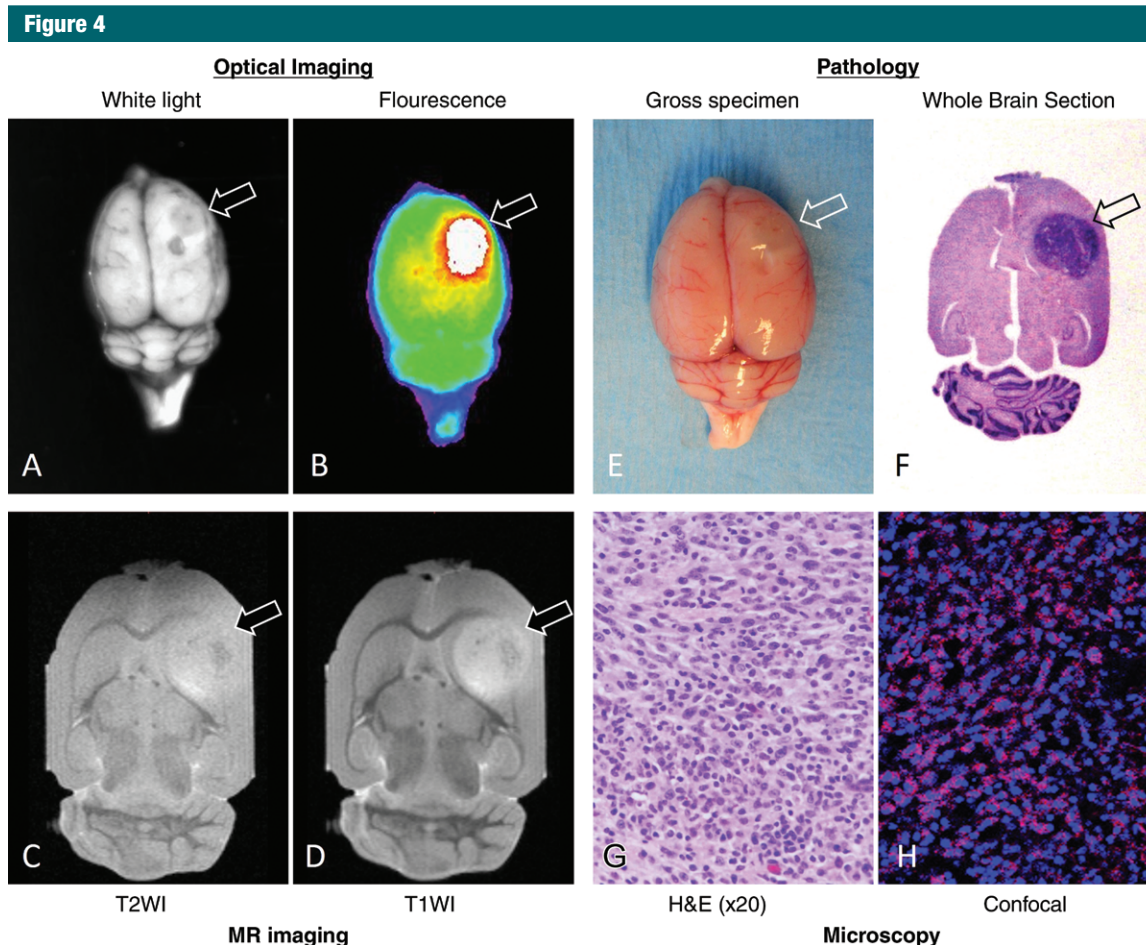


Figure 4: Representative optical and MR images of MGd-enhanced rat glioma mass, with pathologic correlation and confirmation. *A*, Whole-brain white light image of tumor (arrow) and, *B*, overlay image of fluorescent tumor on white-light image clearly show margin of tumor outlined by MGd-emitting fluorescence. *C*, Axial non-contrast-enhanced T2-weighted (*T2WI*) MR image shows tumor with intermediate signal intensity (arrow). *D*, MGd-enhanced T1-weighted (*T1WI*) MR image shows heterogeneous and significant internal enhancement of tumor with clear margin. *E*, Whole-brain photograph displays tumor extruding (arrow) from surface of brain. *F*, Cross-sectional view of hematoxylin and eosin (*H&E*)-stained brain section shows tumor located in frontal caudate area (arrow) and, *G*, glioma tumor is confirmed by means of microscopy. *H*, Confocal microscopic image shows exclusive intracellular accumulation of MGd (pink spots in *H*) in glioma tumor cells.

the tumors. However, the total uptake of MGd was limited. To achieve maximum visibility of tumor margins, continuous intravenous infusion of MGd is necessary to compensate for the gradual loss of MGd from the tumors. Thus, the results of this study are encouraging for the development of an intraoperative imaging technique with MGd as an optical and MR imaging marker to establish the true tumor margin, thereby facilitating the complete removal of gliomas.

Our current animal model had limitations. We could only perform *ex vivo*

imaging of brain tumors from the rat model because of the inherent difficulty in achieving hemostasis at the ruptured cerebral venous sinus in these small animals after craniotomy. This limitation also prevented longitudinal imaging follow-up of each animal. In addition, although we could have performed *in vivo* MR imaging first to evaluate the enhancement patterns of tumors at different time points, this would have been at the expense of optical imaging. During the initial 1–2-hour MR imaging time, MGd might have been cleared from the tumors before optical imaging.

However, the results of our study have established the groundwork that will allow for further advances in commercializing a hybrid imaging modality that integrates both optical and MR imaging. The use of MGd-enhanced intraoperative imaging for precise resection of gliomas will ultimately substantially improve and affect patient care for the population with this challenging condition.

In conclusion, MGd-enhanced optical imaging and molecular MR imaging can allow accurate definition of rat glioma tumor margins within the optimal

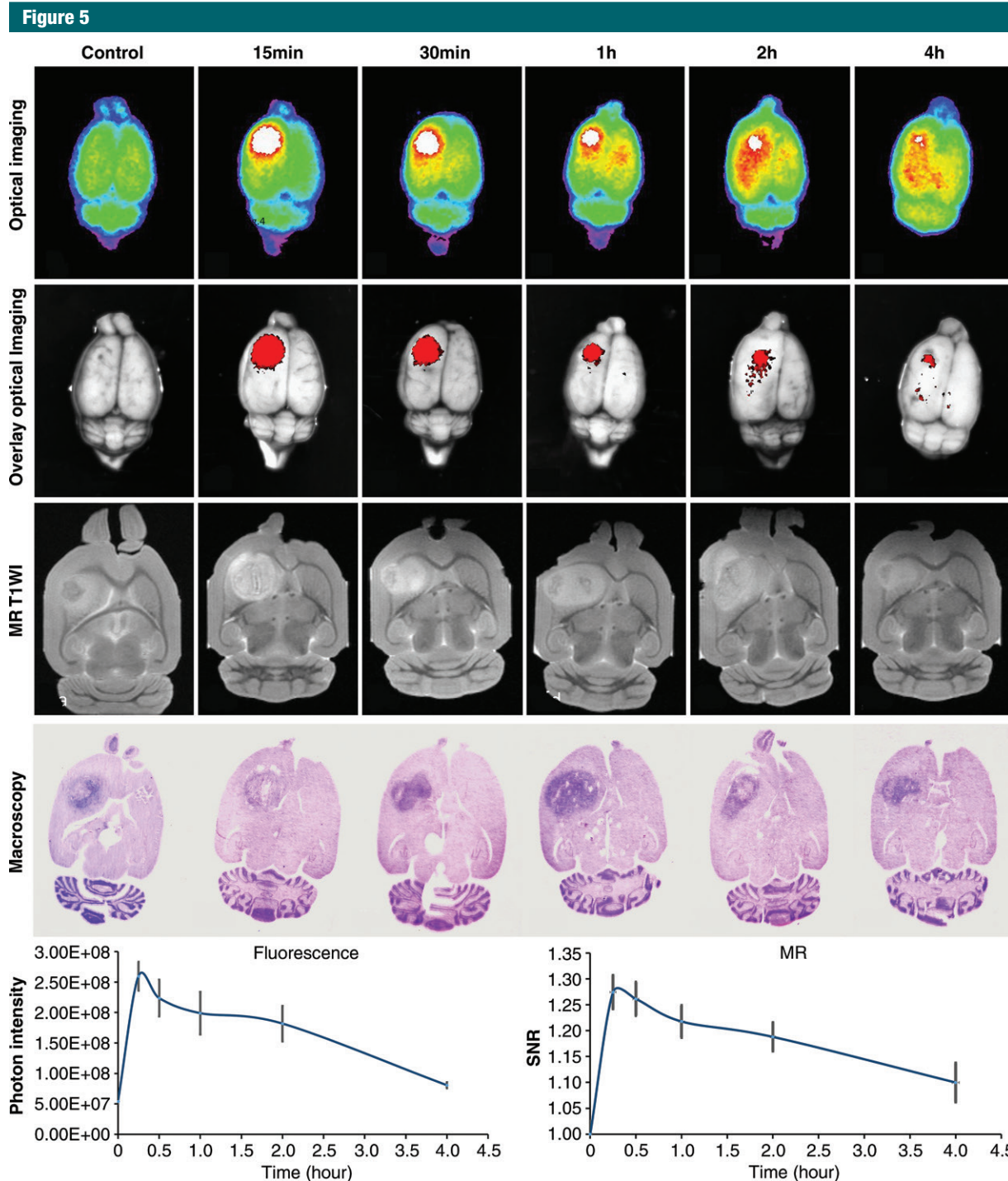


Figure 5: Optical imaging and MGd-enhanced T1-weighted imaging of rat glioma tumors collected at different time points after MGd administration. Optical images (top row) and overlay optical images (second row) show that tumors have highest signal intensity at 15–30 minutes after administration of MGd, and signal intensity becomes weak during observation times of 4 hours. Axial T1-weighted MR images (third row) show strongest enhancement of tumors at 15 minutes, with signal intensity of MGd-enhanced tumors decreasing during observation times. Cross-sectional view of hematoxylin and eosin-stained sections (fourth row) confirms presence of tumors in brains. Graphs show time-to-photon intensity (left) and time-to-signal-to-noise ratio (SNR) curves (right). Steep increase in signal intensity was seen at 15 minutes, followed by gradual signal intensity decline on both optical and MR images. *T1WI* = T1-weighted imaging.

Figure 6

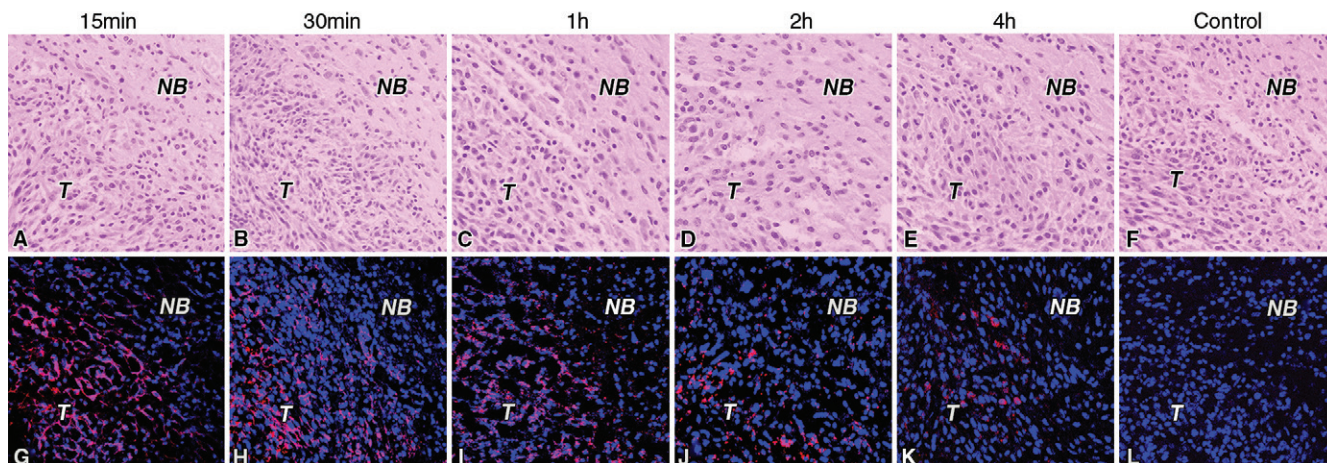


Figure 6: Confocal microscopic images of MGD-treated tumors show that MGD is specifically taken up by glioma cells (intracellular pink spots on G–K), and highest signal intensity is demonstrated at 15 minutes. There is clear margin between MGD-containing tumor cells (T) and normal brain cells (NB).

time window ranging from 15 minutes to 2 hours after MGD administration. These findings present a potential clinical application for complete resection of gliomas in a hybrid surgical setting with intraoperative optical and/or MR imaging.

Acknowledgment: We thank Pharmacyclics for providing motexafin gadolinium.

Disclosures of Conflicts of Interest: L.Q. disclosed no relevant relationships. F.Z. disclosed no relevant relationships. Y.S. disclosed no relevant relationships. Z.B. disclosed no relevant relationships. J.W. disclosed no relevant relationships. Y.L. disclosed no relevant relationships. D.L. disclosed no relevant relationships. C.I. disclosed no relevant relationships. X.F. disclosed no relevant relationships. X.Y. disclosed no relevant relationships.

References

1. Van Meir EG, Hadjipanayis CG, Norden AD, Shu HK, Wen PY, Olson JJ. Exciting new advances in neuro-oncology: the avenue to a cure for malignant glioma. *CA Cancer J Clin* 2010;60(3):166–193.
2. Meyer MA. Malignant gliomas in adults. *N Engl J Med* 2008;359(17):1850; author reply 1850.
3. Eyüpoglu IY, Hore N, Savaskan NE, et al. Improving the extent of malignant glioma resection by dual intraoperative visualization approach. *PLoS One* 2012;7(9):e44885.
4. Stummer W, Pichlmeier U, Meinel T, et al. Fluorescence-guided surgery with 5-aminolevulinic acid for resection of malignant glioma: a randomised controlled multicentre phase III trial. *Lancet Oncol* 2006;7(5):392–401.
5. Colditz MJ, Jeffree RL. Aminolevulinic acid (ALA)-protoporphyrin IX fluorescence guided tumour resection. Part 1: clinical, radiological and pathological studies. *J Clin Neurosci* 2012;19(11):1471–1474.
6. Price SJ, Jena R, Burnet NG, et al. Improved delineation of glioma margins and regions of infiltration with the use of diffusion tensor imaging: an image-guided biopsy study. *AJNR Am J Neuroradiol* 2006;27(9):1969–1974.
7. Wu GN, Ford JM, Alger JR. MRI measurement of the uptake and retention of motexafin gadolinium in glioblastoma multiforme and uninvolved normal human brain. *J Neurooncol* 2006;77(1):95–103.
8. Barone DG, Lawrie TA, Hart MG. Image guided surgery for the resection of brain tumours. *Cochrane Database Syst Rev* 2014; 1:CD009685.
9. Knauth M, Egelhof T, Roth SU, Wirtz CR, Sartor K. Monocrystalline iron oxide nanoparticles: possible solution to the problem of surgically induced intracranial contrast enhancement in intraoperative MR imaging. *AJNR Am J Neuroradiol* 2001;22(1):99–102.
10. Nimsky C. Intraoperative MRI in glioma surgery: proof of benefit? *Lancet Oncol* 2011; 12(11):982–983.
11. Kubben PL, ter Meulen KJ, Schijns OE, ter Laak-Poort MP, van Overbeeke JJ, van Santbrink H. Intraoperative MRI-guided resection of glioblastoma multiforme: a systematic review. *Lancet Oncol* 2011;12(11): 1062–1070.
12. Senft C, Bink A, Franz K, Vatter H, Gasser T, Seifert V. Intraoperative MRI guidance and extent of resection in glioma surgery: a randomised, controlled trial. *Lancet Oncol* 2011;12(11):997–1003.
13. Moiyadi A, Shetty P. Navigable intraoperative ultrasound and fluorescence-guided resections are complementary in resection control of malignant gliomas: one size does not fit all. *J Neurol Surg A Cent Eur Neurosurg* 2014;75(6):434–441.
14. Chi C, Du Y, Ye J, et al. Intraoperative imaging-guided cancer surgery: from current fluorescence molecular imaging methods to future multi-modality imaging technology. *Theranostics* 2014;4(11):1072–1084.
15. Li Y, Rey-Dios R, Roberts DW, Valdés PA, Cohen-Gadol AA. Intraoperative fluorescence-guided resection of high-grade gliomas: a comparison of the present techniques and evolution of future strategies. *World Neurosurg* 2014;82(1-2):175–185.
16. Zhou Z, Chen H, Lipowska M, et al. A dual-modal magnetic nanoparticle probe for preoperative and intraoperative mapping of sentinel lymph nodes by magnetic resonance and near infrared fluorescence imaging. *J Biomater Appl* 2013;28(1):100–111.
17. Stuker F, Baltes C, Dikaiou K, et al. Hybrid small animal imaging system combining magnetic resonance imaging with fluorescence tomography using single photon avalanche diode detectors. *IEEE Trans Med Imaging* 2011;30(6):1265–1273.

18. Hirschberg H, Wu GN, Madsen SJ. Evaluation of Motexafin gadolinium (MGd) as a contrast agent for intraoperative MRI. *Minim Invasive Neurosurg* 2007;50(6):318–323.
19. Meng Y, Wang J, Sun J, et al. 3.0-T MR imaging of intracoronary local delivery of motexafin gadolinium into coronary artery walls. *Radiology* 2013;268(2):556–562.
20. Zhang F, Li J, Meng Y, et al. Development of an intrabiliary MR imaging-monitored local agent delivery technique: a feasibility study in pigs. *Radiology* 2012;262(3):846–852.
21. Wang H, Zhang F, Meng Y, et al. MRI-monitored intra-shunt local agent delivery of motexafin gadolinium: towards improving long-term patency of TIPS. *PLoS One* 2013;8(2):e57419.
22. Brushett C, Qiu B, Atalar E, Yang X. High-resolution MRI of deep-seated atherosclerotic arteries using motexafin gadolinium. *J Magn Reson Imaging* 2008;27(1):246–250.
23. Xu S, Zakian K, Thaler H, et al. Effects of Motexafin gadolinium on tumor metabolism and radiation sensitivity. *Int J Radiat Oncol Biol Phys* 2001;49(5):1381–1390.
24. Miller RA, Woodburn K, Fan Q, Renschler MF, Sessler JL, Koutcher JA. In vivo animal studies with gadolinium (III) texaphyrin as a radiation enhancer. *Int J Radiat Oncol Biol Phys* 1999;45(4):981–989.
25. Sæther CA, Torsteinsen M, Torp SH, Sundstrøm S, Unsgård G, Solheim O. Did survival improve after the implementation of intraoperative neuronavigation and 3D ultrasound in glioblastoma surgery? A retrospective analysis of 192 primary operations. *J Neurol Surg A Cent Eur Neurosurg* 2012;73(2):73–78.
26. Tsugu A, Ishizaka H, Mizokami Y, et al. Impact of the combination of 5-aminolevulinic acid-induced fluorescence with intraoperative magnetic resonance imaging-guided surgery for glioma. *World Neurosurg* 2011;76(1-2):120–127.
27. Zhang Y, Zhang B, Liu F, Luo J, Bai J. In vivo tomographic imaging with fluorescence and MRI using tumor-targeted dual-labeled nanoparticles. *Int J Nanomedicine* 2014;9:33–41.
28. Bradley KA, Zhou T, McNall-Knapp RY, et al. Motexafin-gadolinium and involved field radiation therapy for intrinsic pontine glioma of childhood: a children's oncology group phase 2 study. *Int J Radiat Oncol Biol Phys* 2013;85(1):e55–e60.
29. Meyers CA, Smith JA, Bezjak A, et al. Neurocognitive function and progression in patients with brain metastases treated with whole-brain radiation and motexafin gadolinium: results of a randomized phase III trial. *J Clin Oncol* 2004;22(1):157–165.
30. Richards GM, Mehta MP. Motexafin gadolinium in the treatment of brain metastases. *Expert Opin Pharmacother* 2007;8(3):351–359.